Chemistry and Physics of Lipids 164 (2011) 9–15

Contents lists available at ScienceDirect

Chemistry and Physics of Lipids

journal homepage: www.elsevier.com/locate/chemphyslip

AFM study of the thermotropic behaviour of supported DPPC bilayers with and without the model peptide WALP23

F. Yarrow[a,*], B.W.M. Kuipers[b]

[a] Condensed Matter and Interfaces, Debye Institute for Nanomaterials Science, Science Faculty, Utrecht University, P.O. Box 80000, 3508 TA, Utrecht, The Netherlands
[b] Van 't Hoff Laboratory for Physical and Colloid Chemistry, Debye Institute for Nanomaterials Science, Science Faculty, Utrecht University, P.O. Box 80051, 3508 TB, Utrecht, The Netherlands

ARTICLE INFO

Article history:
Received 27 March 2010
Received in revised form 2 September 2010
Accepted 27 September 2010
Available online 7 October 2010

Keywords:
AFM
Lipid bilayer
Model peptide
Striated phase
Main transition
Grain boundary

ABSTRACT

Temperature-controlled Atomic Force Microscopy (TC-AFM) in Contact Mode is used here to directly image the mechanisms by which melting and crystallization of supported, hydrated DPPC bilayers proceed in the presence and absence of the model peptide WALP23. Melting from the gel $L_{\beta'}$ to the liquid-crystalline L_{α} phase starts at pre-existing line-type packing defects (grain boundaries) in absence of the peptide. The exact transition temperature is shown to be influenced by the magnitude of the force exerted by the AFM probe on the bilayer, but is higher than the main transition temperature of non-supported DPPC vesicles in all cases due to bilayer–substrate interactions. Cooling of the fluid L_{α} bilayer shows the formation of the line-type defects at the borders between different gel-phase regions that originate from different nuclei. The number of these defects depends directly on the rate of cooling through the transition, as predicted by classical nucleation theory.

The presence of the transmembrane, synthetic model peptide WALP23 is known to give rise to heterogeneity in the bilayer as microdomains with a striped appearance are formed in the DPPC bilayer. This striated phase consists of alternating lines of lipids and peptide. It is shown here that melting starts with the peptide-associated lipids in the domains, whose melting temperature is lowered by 0.8–2.0 °C compared to the remaining, peptide-free parts of the bilayer. The stabilization of the fluid phase is ascribed to adaptations of the lipids to the shorter peptide. The lipids not associated with the peptide melt at the same temperature as those in the pure DPPC supported bilayer.

1. Introduction

Phase behaviour of lipid bilayers has been widely investigated for decades using techniques such as DSC, NMR, IR spectroscopy and X-ray diffraction (see for example (Koynova and Caffrey, 2002; McElhaney, 1986; Marsh, 1990)). This has been motivated by the recognition that changes in the physical state of the lipids in the bilayer can play a role in various processes, such as membrane fusion, protein aggregation and functioning (Yeagle, 2005; Lewis and Engelman, 1983). The phase adopted by the lipid bilayer is, amongst others, related to temperature and the chemical composition of the lipid molecules (Yeagle, 2005; Marsh, 1990; Koynova and Caffrey, 2002). A number of phases have been identified in model bilayers of the well-studied phospholipid DPPC, where the higher-temperature phases are characterized by increased lateral and rotational motions of the molecules and a decrease in the order of the hydrocarbon chains with increasing temperature (Yeagle, 2005; Marsh, 1990; Pink et al., 1980). More recently, Atomic Force Microscopy (AFM) has been employed to image the topography of membranes containing various (coexisting) phases. The melting process from the solid, gel $L_{\beta'}$ phase to the fluid L_{α} phase can be followed almost in real-time and allows identification of specific regions where melting or nucleation starts in the presence (Feng et al., 2005) and absence of proteins (Feng et al., 2005; Leonenko et al., 2004; Blanchette et al., 2008; Keller et al., 2005; Garcia-Manyes et al., 2005; Tokumasu et al., 2003). The melting studies on single-component PC bilayers seem to reveal that line-type cracks appear suddenly around the melting temperature T_M.

In the first part of this paper, the thermotropic response of a single supported bilayer of DPPC is studied in detail with Contact-Mode AFM in the heating and cooling direction. It is shown that melting starts at pre-existing line-type packing defects (grain boundaries), whose existence was shown in other studies not concerned with melting behaviour (Rinia et al., 2000; Kim et al., 2003; Hui et al., 1974). It is also shown that cooling at different speeds from the fluid to gel phase affects the number of these grain boundaries. The force exerted by the AFM probe on the bilayer influences

* Corresponding author. Present address: University College Dublin, School of Physics, Belfield, Dublin 4, Ireland. Tel.: +353 1 716 1712; fax: +353 1 283 7275.
E-mail address: fiona.yarrow@ucd.ie (F. Yarrow).

0009-3084/$ – see front matter © 2010 Elsevier Ireland Ltd. All rights reserved.
doi:10.1016/j.chemphyslip.2010.09.007

the measured T_M, something that was not mentioned in previous studies.

The second part of this paper investigates the influence of the model peptide WALP23 on the thermotropic behaviour of the DPPC bilayer. Transmembrane proteins have been shown to affect lipid phase behaviour as they can substantially shift and/or broaden phase transitions and alter the accompanying enthalpy (McElhaney, 1986; Rinia et al., 2002). These effects can be related to adaptations of the system in order to minimize (unfavorable) exposure of hydrophobic parts of the longer species to the hydrophilic environment (De Planque et al., 2003). This leads to stabilization of the best matching lipid phase and hence a shift T_M (McElhaney, 1986).

The synthetic peptide WALP23 has been used successfully to study protein–membrane interactions systematically and has been shown to affect T_M of lipid bilayers in a mismatch-dependent manner (Morein et al., 2002; Rinia et al., 2002). These results can provide insight into interactions in more complex systems, as WALP was designed to mimic one α-helical, hydrophobic transmembrane segment of a multi-spanning protein (Killian et al., 1996). Of special interest is the lateral heterogeneity induced by WALP in otherwise smooth DPPC bilayers as mixed lipid/peptide microdomains with a distinct striated appearance are spontaneously formed (Rinia et al., 2002). The striated pattern is built-up from rows of gel-state lipids with a modified packing, which alternate with single rows of the shorter WALP23 (Sparr et al., 2005). Driving forces are believed to be competing lipid packing effects and lipid–peptide interactions.

It is shown here that AFM can identify differences in melting temperature between the peptide-associated lipids in the striated phase and the peptide-free regions outside the striated domains. It is shown that the shorter WALP23 leads to a stabilization of the thinner fluid phase.

2. Methods and materials

2.1. Preparation of supported bilayers

DPPC (1,2-dipalmitoyl-*sn*-glycero-3-phospocholine) was purchased from Avanti Polar Lipids Inc., Alabaster, USA at >99.0% purity. All used solvents were of analytical grade. NaCl was obtained from Merck (Darmstadt, Germany, p.a. grade). MilliQ-water with a resistivity of >18 MΩ/cm was used throughout. TFE (2,2,2-trifluoroethanol) was from Sigma–Aldrich at 99.5% purity. The model peptide WALP23 was a gift from Prof. J.A. Killian (Dept. Biochemistry of Membranes, Utrecht University). The amino-acid composition of WALP23 is: NH_2–A–W–W–(L–A)$_8$–L–W–W–G–Ac, where A = alanine, W = tryptophan, L = leucine, G = glycine amino acid residues and Ac = acetyl group (Killian et al., 1996).

Supported bilayers (SPBs) were prepared according to the vesicle fusion protocol. First, a dispersion of small unilamellar vesicles (SUVs) was prepared as described in Rinia et al. (2002) with 20 mM NaCl as aqueous phase. Then supported bilayers were prepared by depositing ~75 μl of this SUV dispersion on a clean mica disk (muscovite mica, $KAl_2(OH)_2AlSi_3O_{10}$, regular V-5 sheets PK/10, SPI supplies Structure Probe R, West Chester, USA). A hydrophobic layer around the perimeter of the mica disk prevented the liquid from flowing off. The sample was then heated at 65 °C for 45 min in a sealed container to prevent dehydration and subsequently allowed to cool to room temperature in ~5 min (cooling rate ~10 °C/min, unless stated otherwise, see below). It was rinsed three times with a 20 mM NaCl solution and then placed in the liquid-cell of the AFM to which 0.2–0.3 ml of 20 mM NaCl was added. Care was taken to keep the sample hydrated at all times. All samples were made and measured at least twice to ensure reproducibility. Samples were imaged on the same day of preparing the supported bilayer and within 3 days after vesicle preparation.

The rate by which the sample was cooled after the heating step was varied in some experiments by either turning off the insulated oven and letting it cool to room temperature (cooling rate ~0.6 °C/min) or rinsing it with a 20 mM NaCl solution precooled on ice (~50 °C/min).

2.2. AFM measurements

Samples were imaged by AFM in Contact Mode on a commercial PicoScan Microscope with a S-1286 scanner (Molecular Imaging Corporation, Phoenix, USA, model 305-0002 157) at a scan rate of 3–4 lines/s. Pyramidal shaped Si_3N_4 oxide-sharpened tips mounted on a triangular cantilever with a nominal spring constant of 0.06 N/m and a typical radius of 5–20 nm were used (NP-S, NanoProbe, Digital Instruments Inc., Santa Barbara, USA). A silicon calibration grid that had square ridges with a pitch of 3 μm and step height of 24 nm (TGZ01 UltraSharp grating set, NT-MDT Co., Moscow, Russia) was used for calibration of the AFM scanner. All presented images are in the topographic mode and are background-corrected ('flattened') with the use of the PicoScan 5.2 software (Molecular Imaging). The relative height of the features in the images is represented by a grey scale, where a lighter color indicates a greater height.

The samples were placed on a heating stage for heating above room temperature or a 1× Peltier stage for cooling below room temperature (both Molecular Imaging Corporation, Phoenix, USA). These were coupled to a LakeShore model 330 Temperature Controller. The temperature on top of the sample was found here and by Garcia-Manyes et al. (2005) to deviate from the chosen setpoint temperature, which is measured at the underside of the sample stage. A Pt-100 sensor mounted with a flat metal disk as probe (ø 4.8 mm; Sensycon, Alzenau, Germany) was used to calibrate the temperature on top of the sample while it was immersed in measuring liquid. Calibrated values are used throughout. The error is ~1–2% due to fluctuations of the heater.

Large temperature steps of $\Delta T = 5$ °C were made by stopping the scanning and raising the temperature with a 5 °C/min ramp, followed by a 15-min equilibration period. Smaller temperature steps of $\Delta T = 0.5$–1 °C (ramp rate 5 °C/min) were made around the melting transition (e.g. Figs. 2–4) while the scanning was continued. The force setpoint of the AFM tip was adjusted simultaneously to compensate for the swelling or shrinking of the sample and tip. The sample was monitored for 10–15 min at each temperature to check that no further changes in morphology occurred. The melting transition from the solid gel $L_{\beta'}$ to the fluid, liquid-crystalline L_α phase can be easily recognized by the accompanying reduction in height (Feng et al., 2005; Garcia-Manyes et al., 2005). The temperatures associated with the melting transition of pure DPPC bilayers are defined here by T_{onset} and T_{end}. The former is the lowest temperature where the first traces of fluid phase are observed and the latter the temperature where the fluid phase first covers the whole surface. The onset temperature of the melting in the WALP-containing samples will be denoted by T_{dom} to differentiate from T_{onset} of the WALP-free bilayers.

The thickness of the bilayer is measured as the difference in height between the top of the mica substrate and the top of the bilayer. The symbol d_{gel} denotes the thickness of the gel-state $L_{\beta'}$ bilayer and d_{fluid} that of the fluid L_α state. Both d_{gel} and d_{fluid} were measured through holes piercing the layer. The height difference $\Delta d_{gel-fluid}$ is measured at the border between gel and fluid patches in the coexistence region. Measurements were divided into two categories: those measured with an imaging force F between 0.1 and 0.6 nN and between 0.7 and 0.9 nN. Unfortunately, the relatively

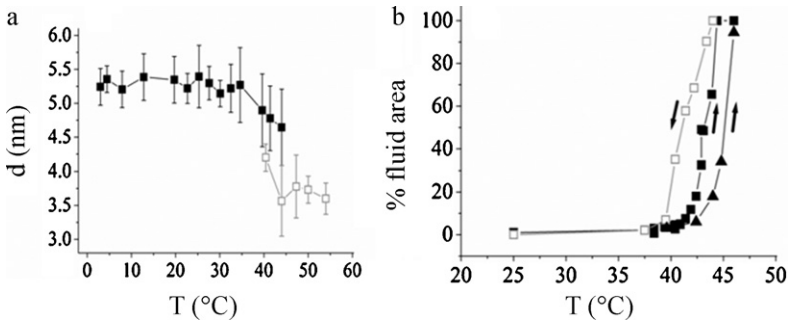

Fig. 1. (a) Thickness of the bilayer d in the gel $L_{\beta'}$ (d_{gel}, ■) and liquid-crystalline L_α phase (d_{fluid}, □) as function of temperature T. (b) Area covered by the L_α phase as function of temperature T: heating scans at low (▲, F = 0.1–0.6 nN) and high (■, F = 0.7–0.9 nN) imaging forces F and cooling scan at F = 0.7–0.9 nN (□).

large error in the measurements did not allow further division beyond these two forces.

Striated domains are present in the WALP23-containing bilayers. These are characterized by a domain height d_{dom} and a repeat distance r_{rep}. The d_{dom} gives the difference in height between the higher, white lines of the striated domains and the top of the surrounding bilayer, while r_{rep} is defined as the distance from one dark stripe to the next. Averages were taken of at least 50 separate measurements. Features provided by the PicoScan 5.2 software (Molecular Imaging Corporation, Phoenix, USA) were used to determine the relative areas of L_α phase.

3. Results

3.1. DPPC bilayers

3.1.1. Melting

The measured thickness d_{gel} of the gel-state DPPC bilayers is given in Fig. 1a (solid squares) and has values of 5.2–5.4 nm between 5 and 35 °C. The surfaces of the bilayers were smooth and relatively featureless (Fig. 2a and b), with occasional holes (black features) and remaining unopened vesicles (white spherical structures). Meandering, dark lines with a depth of ~0.2–0.3 nm were observed at low scanning forces and large magnifications, often bordered by 0.05–0.1 nm high ridges as seen in the close-up in Fig. 2a. These lines are attributed to packing defects; the so-called grain boundaries (see Section 4.1). The surface of the bilayers remained essentially unaltered upon heating to $T \approx 37$ °C, although the holes became progressively smaller and more rounded. The bilayer thickness d_{gel} decreased by ~10–15% above T = 35 °C.

Further heating initially led to a widening of the grain boundaries at T_{onset} as a lower, fluid phase started forming (Fig. 2c). The surface area of the lower, fluid L_α phase expanded at the expense of the higher, gel $L_{\beta'}$ phase (Fig. 2d and e) until it reached 100% at T_{end} (Figs. 1b and 2f). The topographs in Fig. 2 were obtained approximately 5 min after the temperature step, although changes in temperature were immediately reflected upon the morphology and no further changes took place upon repeated imaging during 10–15 min. Consecutive scans could not be made at exactly the same position on the sample due to lateral drift. Some distinctly shaped features, such as V-shaped branches or holes, provided anchoring points by which the relative position of the different images could be determined. These are marked with identical symbols in the scans. The average thickness d_{fluid} was 3.8 ± 0.4 nm, while the average difference $\Delta d_{gel-fluid}$ in the coexistence region was ~0.7 nm.

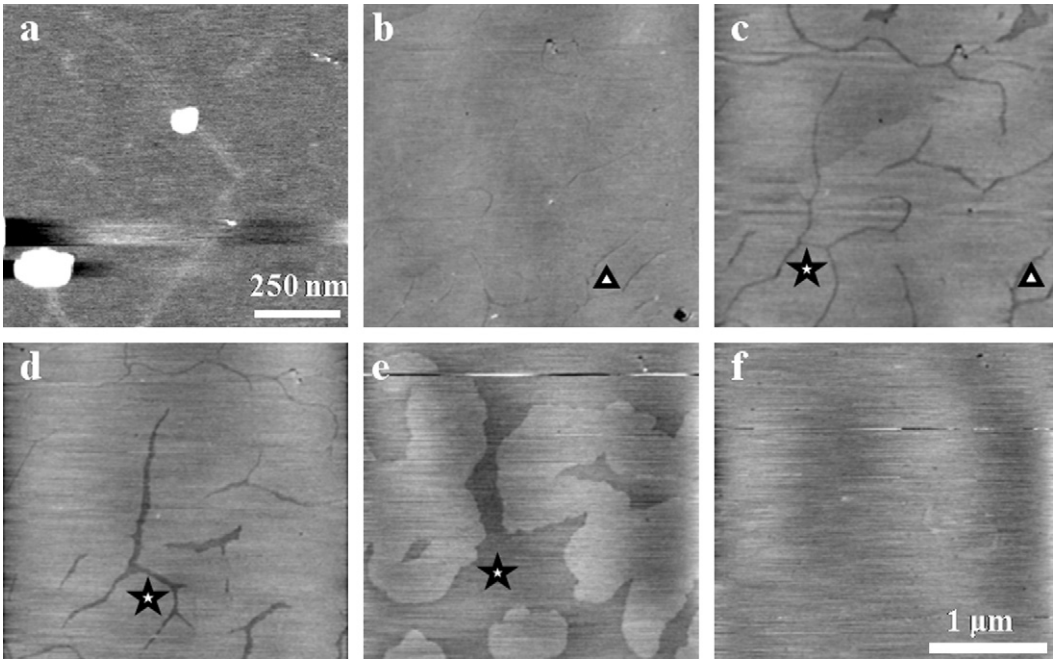

Fig. 2. (a) Close-up of a DPPC bilayer in the gel-state at 25 °C. The grain boundaries are visible as black lines bordered by white lines. (b) Topograph of a supported DPPC bilayer in the gel-state at 39.4 °C showing (very faintly) grain boundaries. The force was slightly higher than in (a) and only black lines are visible as the higher ridges are not imaged. (c–f) Subsequent scans of the area shown in (b) at increasing temperatures: (c) 40.9 °C, (d) 41.9 °C, (e) 43.9 °C and (f) 44.3 °C. (b–f) All have the same lateral scale and a total height (z)-scale of 1 nm, and were recorded at a scanning force F of 0.7–0.9 nN. Identical symbols mark the same characteristic features in the scans.

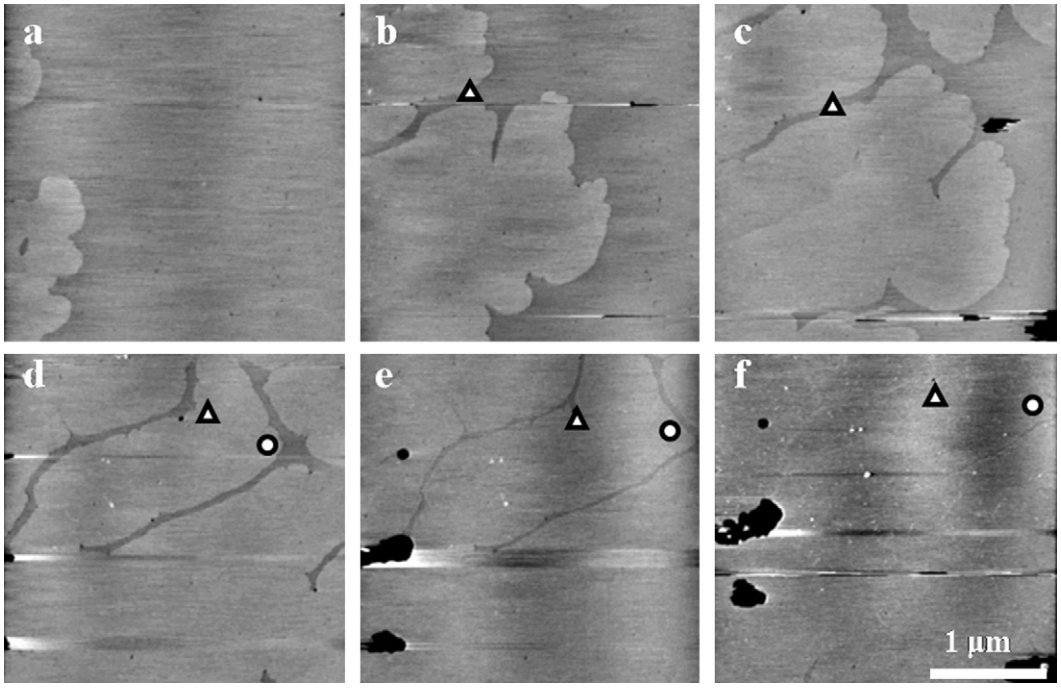

Fig. 3. Subsequent AFM scans of the cooling of a DPPC bilayer at (a) 43.3 °C, (b) 41.4 °C, (c) 40.4 °C, (d) 39.4 °C, (e) 37.5 °C and (f) 35.5 °C. In (f), grain boundaries remain faintly visible as dark lines, often bordered by lighter lines. All images are 3 μm × 3 μm and have a total height scale of ~1 nm.

The exact values of T_{onset} and T_{end} were a function of the applied force F of the AFM probe on the sample (imaging force). A higher F depressed T_{onset} from 42.4 °C (solid triangles in Fig. 1b, F = 0.1–0.6 nN) to 40.4 °C (solid squares, F = 0.7–0.9 nN) and T_{end} from 46.0 °C to 44.4 °C. Extrapolation to zero force leads to crude estimates of $T^0_{onset} \approx 43$ °C and $T^0_{end} \approx 47$ °C.

3.1.2. Crystallization

The reverse process of cooling the L_α DPPC bilayer led to the (random) appearance (Fig. 3a) and growth (Fig. 3b–e) of $L_{\beta'}$ domains. The different solid regions expanded until they touched, leaving line defects at their borders (Fig. 3f). Holes appeared and expanded during the cooling process. The cooling curve in Fig. 1b (open squares) showed a pronounced hysteresis of ~2–3 °C with the heating curve.

The number of line defects was enhanced by a faster cooling rate, with the cumulative length of these lines per area unit increasing from approximately 1 μm/μm^2 at 0.6 °C/min, 3 μm/μm^2 at 10 °C/min to 5 μm/μm^2 at 50 °C/min. The number of holes and lipid debris also increased with the cooling rate.

3.2. Mixed DPPC/WALP23 bilayers

3.2.1. Melting

Previous AFM studies have shown that DPPC bilayers with 2 mol% WALP23 contain domains that are elevated with respect to the surrounding pure DPPC bilayer (Fig. 4a, with the inset showing the stripes in detail)). The properties of these striated domains in the gel phase have been studied previously on supported and unsupported bilayers. Gold-labeling, X-ray diffraction and fluorescence measurements proved that the lighter stripes are rows of lipids with a modified packing, which alternate with single rows of the shorter WALP23 in a 8:1–10:1 ratio (Rinia et al., 2002; Sparr et al., 2005).

Heating of 2 mol% WALP23/DPPC bilayers from 8 to 35 °C did not lead to changes in the striped organization, as the spacing r_{rep} continued to be around 7.7 (±0.5) nm and the domain height d_{dom} around 0.3–0.4 nm (Fig. 5) between T = 3–25 °C. d_{dom} was slightly reduced between 25 and 35 °C. Further heating above T = 35 °C led to a 'sinking-in' of the previously higher domains at T_{dom}, as shown in Fig. 4b and c. The lesser quality of the gel phase domain in Fig. 4b is due to a relatively high F and softening of the layer at

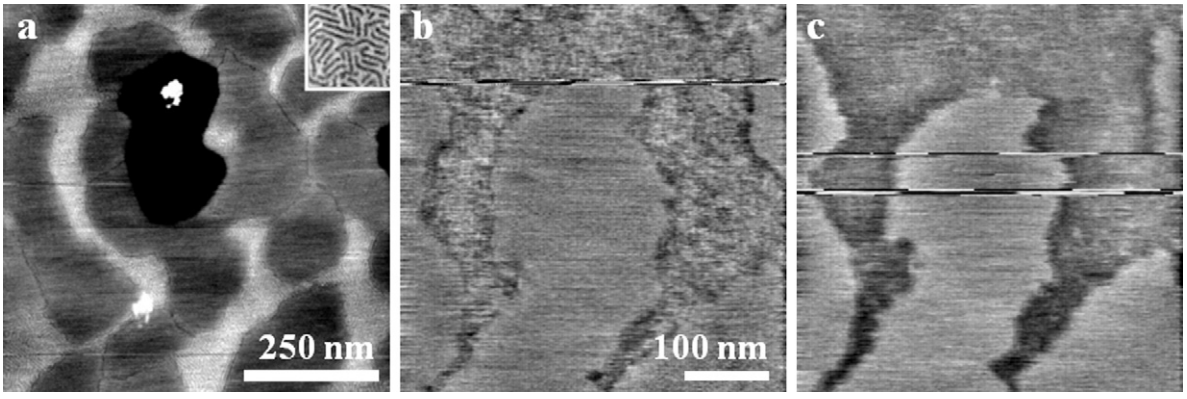

Fig. 4. (a) Topography image of a WALP23/DPPC bilayer in the gel phase at 25.3 °C, where striated domains are visible as lighter domains. The inset shows a 100 nm × 100 nm close-up of the striated phase. (b) One striated region before melting at 38.5 °C, imaged at relatively high F and (c) the same region after melting at 40.3 °C.

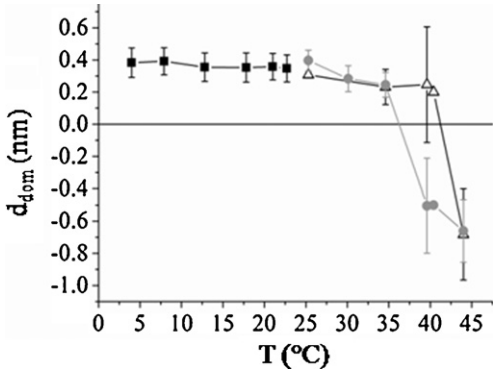

Fig. 5. Domain height d_{dom} as function of temperature T. The initial part of the graph is for all forces $F = 0.1–0.9$ nN (■), while in the second half the data were split into low ($F = 0.1–0.6$ nN, Δ) and high force ($F = 0.7–0.9$ nN, ●).

Table 1
Effect of cooling rate upon the diameter of the striated domains, domain height d_{dom} and repeat distance r_{rep}.

Cooling rate (°C/min)	Length scale of domains (nm)	d_{dom} (nm)	r_{rep} (nm)
0.6	801 ± 262	0.4 ± 0.1	7.8 ± 0.6
10	285 ± 119	0.3 ± 0.1	7.7 ± 0.5
50	63 ± 23	0.3 ± 0.1	7.7 ± 0.5

the used temperature. The transition is regarded as melting of the lipids in the domains (see Section 4.2). The exact value of T_{dom} was again force-dependent and varied from $T_{dom} = 40.4$ °C at low forces of $F \approx 0.1–0.6$ nN to 39.6 °C at relatively high scanning forces of $F \approx 0.7–0.9$ nN.

The bilayer area outside the domains melted around a higher ~44 °C at low F, when the fluid phase expanded from the molten domains outwards.

3.2.2. Crystallization

Striated domains reappeared unaltered with $r_{rep} = 7.9 \pm 0.4$ nm and $d_{dom} = 0.4 \pm 0.1$ nm upon returning the sample to room temperature after the heating step. A faster cooling rate led to smaller, more intercalated domains and more holes (see Table 1).

4. Discussion

4.1. DPPC bilayers

4.1.1. Melting

The measured values for d_{gel} of ~5.2–5.4 nm in the gel phase are slightly lower, but in reasonable agreement with reported values from AFM of 5.8–5.9 nm (Rinia et al., 2000) and 5.6 nm (Mou et al., 1996). Differences in applied scanning force, pH or ionic strength could account for the slight differences. The observed reduction at $T > 37$ °C is probably related to mechanical changes of the bilayer (Garcia-Manyes et al., 2005), making it softer and thus more susceptible to indentation by the scanning tip. The fluid or liquid-crystalline L_α phase which appears above T_{onset} has a thickness d_{fluid} of 3.8 ± 0.4 nm. This is comparable to the 3.6 nm (Tokumasu et al., 2003) and 3.3 nm (Leonenko et al., 2004) of other AFM studies. d_{fluid} is probably underestimated in all these AFM studies as the scanning probe will deform and/or penetrate partially into the layer of flexible lipids.

The scans in Fig. 2a and b show that melting starts at the line-type packing defects that were already present below T_{onset}. These grain boundaries separate domains with a different crystal orientation. The interrupted packing provides a convenient starting place for melting as the fluid lipids require additional space within the tightly-packed gel state bilayer due to the disordering of their chains and related expansion of their in-plane molecular (Yeagle, 2005; Marsh, 1990). Surface melting in bilayers was already observed at edges of differently oriented lipid domains in the ripple phase (Leidy et al., 2002) and was predicted theoretically by computer simulations (Zuckermann and Mouritsen, 1987). Line defects in the gel phase were not mentioned or shown in the (large-scale) images in Feng et al. (2005), Garcia-Manyes et al. (2005), and Tokumasu et al. (2003) of similar single-component bilayers, where cracks of fluid phase seem to appear suddenly around T_{onset}. It is shown in Fig. 2 that these cracks originate from pre-existing line defects instead of appearing randomly. The fact that we do observe grain boundaries in a one-component gel-phase bilayer might be related to the smaller scale of our images or the use of Contact Mode, where the AFM probe could artificially 'stretch' the grain boundaries and enhance their visibility. Other AFM studies that did not regard melting, but showed these grain boundaries also employed Contact Mode (Rinia et al., 2000; Mou et al., 1996). Other techniques have also shown the presence of line-defects, i.e. Brewster angle microscopy (Weidemann and Vollhardt, 1995), Electron Microscopy (Kim et al., 2003) and electron diffraction (Hui et al., 1974).

Further growth from the fluid cracks outwards proceeds through a pattern that is similar to the ones in Feng et al. (2005) and Tokumasu et al. (2003), indicating that line-defects were probably present but not observed there in the gel phase.

The melting transition for supported bilayers is higher than that for unsupported bilayers ($T_M = 41$ °C (Marsh, 1990)), as was previously demonstrated in AFM and DSC studies (Yang and Appleyard, 2000; Feng et al., 2005). Interactions between the polar PC groups and the mica substrate are believed to lead to the observed increase in T_M and reduced cooperativity, as well as to the observed hysteresis between the heating and cooling curve. The same bilayer-mica interactions are believed to give a decoupling between the proximate, substrate-bordering and the distal leaflet (Yang and Appleyard, 2000; Feng et al., 2005; Garcia-Manyes et al., 2005; Keller et al., 2005). The second transition associated with the melting of the separate leaflets in these studies was not observed here, however. This might be due to differences in experimental details (e.g. salt concentration).

4.1.2. Effect of force on the transition

The melting transition is largely completed between 42.4 and 46 °C at low F (or between 43 and 47 °C when extrapolated to zero imaging force). Other AFM studies have reported ranges of 41–45.5 °C (Feng et al., 2005), 42–52 °C (Leonenko et al., 2004) and 44.8–51.5 °C (Garcia-Manyes et al., 2005) for supported DPPC bilayers. The differences can probably be attributed to experimental variations in heating rate, ionic strength, equilibration time and imaging force. The imaging force has a considerable influence on the melting temperature, as shown in Fig. 1. This is presumably due to axial compression of lipids with a modified, somewhat fluidized packing in the immediate vicinity of the gel–fluid borders (Akimov et al., 2004). The AFM probe most likely pushes these L_β' lipids down at higher F, which creates an apparent T_{onset} and T_{end} below the 'real' T^0_{onset} and T^0_{end} at zero force. The use of the intermittent-contact modes in Feng et al. (2005), Leonenko et al. (2004) and Tokumasu et al. (2003) does not prevent axial forces being exerted on the bilayer, so T_M could be shifted in these studies as well. This is the first time a correlation between T_M and imaging force F has been reported.

4.1.3. Crystallization

The random distribution of the gel-phase nuclei that appear in the fluid phase upon cooling indicates homogeneous nucleation (Blanchette et al., 2008). After growth of the nuclei and complete solidification, borders (grain boundaries) remain at the edges of the individual domains. These are borders between domains that

have a different orientation of the lipids as the azimuth angle of the tilted lipids in each nucleus will vary (Rinia et al., 2000). This angle is subsequently adopted by the lipids that attach to the nucleus during growth, leading to differently oriented domains that do not seal into a continuous layer.

The relationship between total number of boundary lines and the cooling rate is governed by the kinetics of the transition. Classical nucleation theory predicts that the size of the formed nuclei is related to the degree of undercooling (=T_M – actual temperature) of the system. A faster rate of cooling leads to a larger undercooling during the nucleation step, which was found to take approximately 1 min for a comparable supported DSPC bilayer (Blanchette et al., 2008). This will lead to more and smaller nuclei, as also shown in (Blanchette et al., 2008). This will eventually give a larger number of continuous crystalline patches with a smaller size and, hence, more boundary lines. A similar dependency between domain size and cooling rate has been observed for DSPC monolayers (Kim et al., 2003) and DPPC bilayers (Hui et al., 1974) with other techniques.

4.2. Mixed DPPC/WALP23 bilayers

4.2.1. Melting

Both the striated domains and the surrounding bilayer remain essentially unaltered between 8 and 39 °C. The small reduction of d_{dom} is likely to be due to mechanical softening of the bilayers (Garcia-Manyes et al., 2005; Heimburg, 1998). Melting starts with the disappearance of the higher WALP-containing domains at T_{dom} = 40.4 °C (low F). The final difference in height between the sunken-in, molten domains and the unperturbed gel-state bilayer is 0.5–0.7 nm, which matches $\Delta d_{gel-fluid}$ of the previous section. It can therefore be concluded that the sinking-in of the domains is caused by melting of the lipids within the domains from their predominantly gel-like phase to the fluid phase. WALP23 itself is expected to be unaffected by temperature and retain its α-helical conformation (Killian et al., 1996).

The striated domains consist of single rows of WALP23 alternating with lipids that have a modified packing due to the presence of the peptide (Sparr et al., 2005). The peptide-associated lipids in the domains melt ∼2.0 °C lower (at low F) than those in the pure DPPC bilayers. DSC thermograms of WALP23/DPPC liposomes showed a comparable reduction of T_{onset} by 1.8 °C and of T_M by 0.8 °C (Rinia et al., 2002). Other studies corroborate that WALP can shift T_M in a manner that correlates to the hydrophobic length of the peptide (De Planque et al., 2003; Morein et al., 2002). The length of the hydrophobic stretch of WALP23 of 2.6 nm (De Planque et al., 2003) is closer to the hydrophobic thickness of the thinner L_α phase (2.6 nm (Dumas et al., 1999)) than to the $L_{\beta'}$ state (3.3–3.6 nm (Dumas et al., 1999)), leading to a stabilization of the fluid phase, and hence, a reduction in T_M. Stabilization of the phase with the closest matching hydrophobic length has been encountered in a number of other protein/lipid systems with other techniques, such as DSC (Dumas et al., 1999; Papahadjopoulos et al., 1975).

The lipids outside the molten WALP23/lipid domains are not affected by the peptide and melt at the same temperature as the lipids in the pure DPPC bilayers.

The less rigid packing in the fluid phase leads to a higher solubility of the peptide in the lipid layer (Sparr et al., 2005). Fluorescence spectroscopy (Sparr et al., 2005) and ESR measurements (De Planque et al., 1998) indicated disaggregation of WALP upon entering the less-rigidly packed L_α phase. This leads to the removal of the rigid striated ordering. Any changes in the morphology of the striated domains at T_{onset} can unfortunately not be clearly discerned as the length of the peptide is too close to that of the soft L_α lipid phase. However, careful inspection in the region just below T_{onset} at low F reveals an irregular pattern (Fig. 6), which could be caused by disordering or partial disaggregation of the lines of peptide. Disaggregation in response to an altered lipid packing mode has been also encountered for a number of other proteins through fluorescent energy transfer, e.g. the pulmonary surfactant protein SP-C (Horowitz et al., 1993) and bacteriorhodopsin (Hasselbacher et al., 1984).

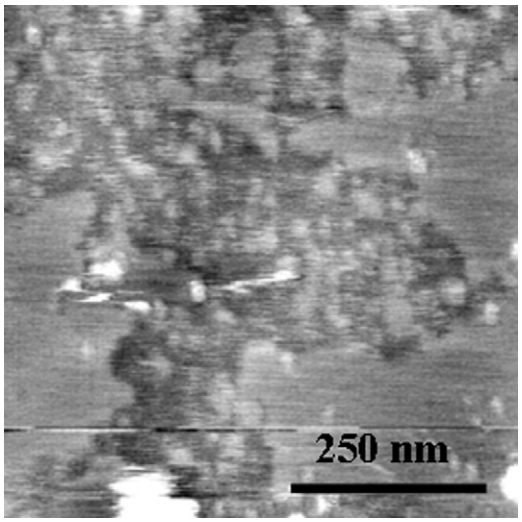

Fig. 6. Intermediate structure found near the onset of melting at 40 °C (at low F).

The transmembrane peptide gramicidin A forms a somewhat similar pattern in DPPC bilayers as WALP does (Mou et al., 1996) and is expected to show similar melting behaviour. However, no pattern was observed in an AFM study concerning the melting behaviour of a gramicidin/DMPC system (Feng et al., 2005). Only lower-lying, structureless domains were observed, which are believed to contain the gramicidin. Melting seems a gradual process from these domains outwards and no difference between peptide associated and non-associated lipids was reported, although T_M of the whole system was lowered slightly by ∼2 °C. This seems to contradict our study. The gramicidin-rich domains in Feng et al. (2005), however, resemble images of compressed WALP/DPPC striated domains at high scanning forces of 1.5 nN (Rinia et al., 2000), so these results might be due to influence of the scanning probe. Alternatively, their use of a different buffer (phosphate buffer) might lead to differences in the melting behaviour or appearance of these systems (Cunningham et al., 1986).

4.2.2. Crystallization

Striated domains with identical characteristics reappear upon returning to the gel phase. The low solubility of WALP in the gel phase leads to its expulsion from the growing solid areas to the grain boundaries or to striated domains that are formed at positions where several grain boundaries meet. The size of the striated domains is inversely proportional to the cooling rate, as slower cooling leads to less nuclei, larger areas of unperturbed DPPC bilayer, and, in consequence, larger striated domains. A qualitatively similar effect was observed by Rinia et al. (2000) for these systems. The rate of cooling does not affect the underlying physical interactions of the stripe formation as evidenced by the constant r_{rep} and d_{dom}.

5. Conclusions

The advantage of a direct technique like AFM in the study of lipid phase behaviour is evident from the presented results. Membrane regions have been identified that act as specific starting points for melting from the gel $L_{\beta'}$ to the liquid-crystalline L_α phase; something not possible with DSC. Melting in supported model

membranes of pure DPPC starts at pre-existing grain boundaries where the crystal packing is perturbed. All measured transition temperatures are lowered as the force exerted by the AFM probe increases. This underlines the importance of minimizing the imaging force in the study of thermal transitions with AFM and could be the source for the deviations in melting temperatures between the different AFM studies.

The reverse process of solidification of a DPPC bilayer from the $L_\alpha \rightarrow L_{\beta'}$ phase starts with the formation of small gel-state nuclei that grow until regions are formed that are separated by line defects. The lipids in each different solid region are expected to have different azimuth angles, but similar polar angles. Faster cooling rates lead to a substantial increase of these line defects. This is in line with classical nucleation theory, where an increase in the number of nuclei and hence increase in the number of grain boundaries is predicted under these circumstances.

In the mixed bilayers of WALP/DPPC, striated domains are formed where the conformation of the lipids is affected by the peptide. The lipids in the striped phase melt 1–2 °C lower than those in the surrounding WALP-free bilayer. This can be explained by stabilization of the better-matching, shorter fluid phase of the lipids that are in contact with the peptide. Some dispersal of the lines of WALP seems to occur just below T_M, in agreement with the almost complete disaggregation of WALP found in fluorescence studies (Sparr et al., 2005). This indicates the importance of the lipid environment on the lateral distribution of the peptides. Striated domains with identical properties reappear upon cooling from the $L_\alpha \rightarrow L_{\beta'}$ phase at all used rates of cooling. This points to a general and speed-independent underlying mechanism for their formation. Their size, however, is inversely proportional to the cooling rate.

Acknowledgments

This research was funded by the Netherlands Organization for Scientific Research (NWO). Thanks to Prof. Dr. J.A. Killian for providing the WALP and Pa-WALP and to Prof. Dr. B. de Kruijff for useful discussions.

References

Akimov, S.A., Kuzmin, P.I., Zimmerberg, J., Cohen, F.S., Chizmadzhev, Y.A., 2004. An elastic theory for line tension at a boundary separating two lipid monolayer regions of different thickness. J. Electroanal. Chem. 564, 13–18.

Blanchette, C.D., Lin, W.-C., Orme, C.A., Ratto, T.V., Longo, M.L., 2008. Quantifying growth of symmetric and asymmetric lipid bilayer domains. Langmuir 24, 1219–1224.

Cunningham, B.A., Shimotake, J.E., Tamura-Lis, W., Mastran, T., Kwok, W.-M., Kauffman, J.W., Lis, L.J., 1986. The influence of ion species on phosphatidylcholine bilayer structure and packing. Chem. Phys. Lipids 39, 135–143.

De Planque, M.R.R., Bonev, B.B., Demmers, J.A.A., Greathouse, D.V., Koeppe I.I., R.E., Separovic, F., Watts, A., Killian, J.A., 2003. Interfacial anchor properties of tryptophan residues in transmembrane peptides can dominate over hydrophobic matching effects in peptide-lipid interactions. Biochemistry 42, 5341–5348.

De Planque, M.R.R., Greathouse, D.V., Koeppe I.I., R.E., Separovic, F., Watts, A., Killian, J.A., 1998. Influence of lipid/peptide hydrophobic mismatch on the thickness of diacylphosphatidylcholine bilayers. A 2H NMR and ESR study using designed transmembrane α-helical peptides and gramicidin A. Biochemistry 37, 9333–9345.

Dumas, F., Lebrun, M.-C., Tocanne, J.-F., 1999. Is the protein/lipid hydrophobic matching principle relevant to membrane organization and functions? FEBS Lett. 458, 271–277.

Feng, Z.V., Spurlin, T.A., Gewirth, A.A., 2005. Direct visualization of asymmetric behavior in supported lipid bilayers at the gel–fluid phase transition. Biophys. J. 88, 2154–2164.

Garcia-Manyes, S., Oncins, G., Sanz, F., 2005. Effect of temperature on the nanomechanics of lipid bilayers studied by Force Spectroscopy. Biophys. J. 89, 4261–4274.

Hasselbacher, C.A., Street, T.L., Dewey, T.G., 1984. Resonance energy transfer as a monitor of membrane protein domain segregation: application to the aggregation of bacteriorhodopsin reconstituted into phospholipid vesicles. Biochemistry 23, 6445–6452.

Heimburg, T., 1998. Mechanical aspects of membrane thermodynamics. Estimation of the mechanical properties of lipid membranes close to the chain melting transition from calorimetry. Biochim. Biophys. Acta 1415, 147–162.

Horowitz, A.D., Baatz, J.E., Whitsett, J.A., 1993. Lipid effects on aggregation of pulmonary surfactant protein SP-C studied by fluorescence energy transfer biochemistry. Biochemistry 32, 9512–9523.

Hui, S.W., Parsons, D.F., Cowden, M., 1974. Electron diffraction of wet phospholipid bilayers. Proc. Natl. Acad. Sci. U. S. A. 71, 5068–5072.

Keller, D., Larsen, N.B., Møller, I.M., Mouritsen, O.G., 2005. Decoupled phase transitions and grain-boundary melting in supported phospholipid bilayers. Phys. Rev. Lett. 94, 025701.

Killian, J.A., Salemink, I., De Planque, M.R.R., Lindblom, G., Koeppe, R.E.II., Greathouse, D.V., 1996. Induction of nonbilayer structures in diacylphosphatidylcholine model membranes by transmembrane α-helical peptides: importance of hydrophobic mismatch and proposed role of tryptophans. Biochemistry 35, 1037–1045.

Kim, D.H., Costello, M.J., Duncan, P.B., Needham, D., 2003. Mechanical properties and microstructure of polycrystalline phospholipid monolayer shells: novel solid microparticles. Langmuir 19, 8455–8466.

Koynova, R., Caffrey, M., 2002. An index of lipid phase diagrams. Chem. Phys. Lipids 115, 107–219.

Leidy, C., Kaasgaard, T., Crowe, J.H., Mouritsen, O.G., Jørgensen, K., 2002. Ripples and the formation of anisotropic lipid domains: imaging two-component supported double bilayers by Atomic Force Microscopy. Biophys. J. 83, 2625–2633.

Leonenko, Z.V., Finot, E., Ma, H., Dahms, T.E.S., Cramb, D.T., 2004. Investigation of temperature-induced phase transitions in DOPC and DPPC phospholipid bilayers using temperature-controlled Scanning Force Microscopy. Biophys. J. 86, 3783–3793.

Lewis, B.A., Engelman, D.M., 1983. Bacteriorhodopsin remains dispersed in fluid phospholipid bilayers over a wide range of bilayer thicknesses. J. Mol. Biol. 166, 203–210.

Marsh, D., 1990. CRC Handbook of Lipid Bilayers. CRC Press Inc, Boca Raton, USA.

McElhaney, R.N., 1986. The use of differential scanning calorimetry and differential thermal analysis in studies of model and biological membranes. Biochim. Biophys. Acta 864, 361–421.

Morein, S., Killian, J.A., Sperotto, M.M., 2002. Characterization of the thermotropic behavior and lateral organization of lipid–peptide mixtures by a combined experimental and theoretical approach: effects of hydrophobic mismatch and role of flanking residues. Biophys. J. 82, 1405–1417.

Mou, J., Czajkowsky, D.M., Shao, Z., 1996. Gramicidin A aggregation in supported gel state phosphatidylcholine bilayers. Biochemistry 35, 3222–3226.

Papahadjopoulos, D., Moscarello, M., Eylar, E.H., Isac, T., 1975. Effects of proteins on the thermotropic phase transitions of phospholipid membranes. Biochim. Biophys. Acta 401, 317–335.

Pink, D.A., Green, T.J., Chapman, D., 1980. Raman scattering in bilayers of saturated phosphatidylcholines. Experiment and theory. Biochemistry 19, 349–356.

Rinia, H.A., Boots, J.W.P., Rijkers, D.T.S., Kik, R.A., Demel, R.A., Snel, M.M.E., Killian, J.A., Van der Eerden, J.P.J.M., De Kruijff, B., 2002. Domain formation in phosphatidylcholine bilayers containing transmembrane peptides: specific effects of flanking residues. Biochemistry 41, 2814–2824.

Rinia, H.A., Kik, R.A., Demel, R.A., Snel, M.M.E., Killian, J.P.J.M., Van der Eerden, J.A., De Kruijff, B., 2000. Visualization of highly ordered striated domains induced by transmembrane peptides in supported phosphatidylcholine bilayers. Biochemistry 39, 5852–5858.

Sparr, E., Ganchev, D.N., Snel, M.M.E., Ridder, A.N.J.A., Kroon-Batenburg, L.M.J., Chupin, V., Rijkers, D.T.S., Killian, J.A., De Kruijff, B., 2005. Molecular organization in striated domains induced by transmembrane α-helical peptides in dipalmitoyl phosphatidylcholine bilayers. Biochemistry 44, 2–10.

Tokumasu, F., Jin, A.J., Feigenson, G.W., Dvorak, J.A., 2003. Atomic force microscopy of nanometric liposome adsorption and nanoscopic membrane domain formation. Ultramicroscopy 97, 217–227.

Weidemann, G., Vollhardt, D., 1995. Long-range tilt orientational order in phospholipid monolayers: the inner structure of dimyristoyl-phosphatidylethanolamine domains. Thin Solid Films 264, 94–103.

Yang, J., Appleyard, J., 2000. The main phase transition of mica-supported phosphatidylcholine membranes. J. Phys. Chem. B 104, 8097–8100.

Yeagle, P.L., 2005. The Structure of Biological Membranes. CRC Press, Boca Raton, USA.

Zuckermann, M.J., Mouritsen, O.G., 1987. An elastic theory for line tension at a boundary separating two lipid monolayer regions of different thickness. Eur. Biophys. J. 15, 77–86.